

Accepted Manuscript

Optimising the locations of thermally sensitive equipment in an aircraft crown compartment

C. Butler, D. Newport, M. Geron

PII: S1270-9638(12)00204-0
DOI: [10.1016/j.ast.2012.12.005](https://doi.org/10.1016/j.ast.2012.12.005)
Reference: AESCTE 2872

To appear in: *Aerospace Science and Technology*

Received date: 17 April 2012
Revised date: 30 November 2012
Accepted date: 13 December 2012

Please cite this article in press as: C. Butler et al., Optimising the locations of thermally sensitive equipment in an aircraft crown compartment, *Aerospace Science and Technology* (2012), <http://dx.doi.org/10.1016/j.ast.2012.12.005>

This is a PDF file of an unedited manuscript that has been accepted for publication. As a service to our customers we are providing this early version of the manuscript. The manuscript will undergo copyediting, typesetting, and review of the resulting proof before it is published in its final form. Please note that during the production process errors may be discovered which could affect the content, and all legal disclaimers that apply to the journal pertain.



Optimising the locations of thermally sensitive equipment in an aircraft crown compartment

C. Butler^a, D. Newport^{a,*}, M. Geron^{b,1}

^aStokes Institute, Dept. of Mechanical, Aeronautical & Biomedical Engineering, University of Limerick, Limerick, Ireland

^bDept. of Civil Engineering, National University of Ireland Galway, Galway, Ireland

Abstract

A Design of Experiments (DoE) analysis was undertaken to generate a list of configurations for CFD numerical simulation of an aircraft crown compartment. Fitted regression models were built to predict the convective heat transfer coefficients of thermally sensitive dissipating elements located inside this compartment. These are namely the SEPDC and the Route G. Currently they are positioned close to the fuselage and it is of interest to optimise the heat transfer for reliability and performance purposes. Their locations and the external fuselage surface temperature were selected as input variables for the DoE. The models fit the CFD data with R^2 values ranging from 0.878 - 0.978, and predict that the optimum locations in terms of heat transfer are when the elements are positioned as close to the crown floor as possible (S_y and $R_y \rightarrow \min.$ limits), where they come in direct contact with the air flow from the cabin ventilation system, and when they are positioned close to the centreline (S_x and $R_x \rightarrow \text{CL}$).

The methodology employed allows aircraft thermal designers to optimise equipment placement in confined areas of an aircraft during the design phase. The determined models should be incorporated into global aircraft numerical models to improve accuracy and reduce model size and computational time.

Keywords: aircraft compartment, heat transfer, thermal management, design of experiments

1. Introduction

The next generation of modern commercial aircraft are including greater levels of composite materials in their design, with both Airbus and Boeing citing up to 50% composite in their next generation aircraft: A350 53% and 787 50% [12]. Substantial attention has been given to their strength, manufacture, fatigue and impact properties for aviation [5, 20, 25], with only minimal attention being devoted to the thermal impact that arises from their use [7]. The very low thermal conductivity of composite materials relative to aluminium means that the thermal environment experienced in aircraft compartments during flight and on the apron can lead to critical systems experiencing elevated ambient temperatures, possibly compromising reliability and safety of the aircraft.

The majority of work published to date dealing with aircraft compartments has focused on the environment in the main passenger cabin to improve comfort and to reduce the risk of the spread of airborne pathogens amongst passengers. Günther et al. [10] presented a numerical and

experimental comparison of the thermal and flow fields in two different cabins of a modern mega airliner. Kühn et al. [14] investigated the forced and mixed convection in an Airbus A380 passenger cabin by experimental means. It was found that the flow field is affected by various fluid mechanical phenomena such as interaction of fluid jets and negative buoyancy forces. Bianco et al. [6] numerically studied the thermal and fluid dynamic fields in the cabin of an executive aircraft and achieved good agreement between their 2- and 3D models. Mellert et al. [16] investigated the effect of the cabin environmental conditions such as noise, vibration, air quality and temperature distribution on the health and performance of cabin and flight crew. Gupta et al. [11] conducted a numerical investigation on the transportation of infectious droplets exhaled by a passenger in a fully occupied aircraft cabin. It was found that the airflow pattern in the cabin played a significant role on the droplet transportation and the droplets were dispersed uniformly to all surrounding rows in 4 minutes. A summary of previous works dealing with cabin air distributions to the date of its publication is given by Liu et al. [15].

A recent study by Moore et al. [18] has focused on the heat transfer in the confined area inside the leading edge of an aircraft's wing. The experimental enclosure was heated on its external surface, contained an internal heat source and included ventilation slots. The location of a partition inside the compartment and the vent orientation

*Corresponding author. Tel.: +353 61 202849; Fax: +353 61 202393

Email addresses: colin.butler@ul.ie (C. Butler), david.newport@ul.ie (D. Newport), marco.geron@nuigalway.ie (M. Geron)

¹Work conducted in Stokes Institute but current affiliation has changed

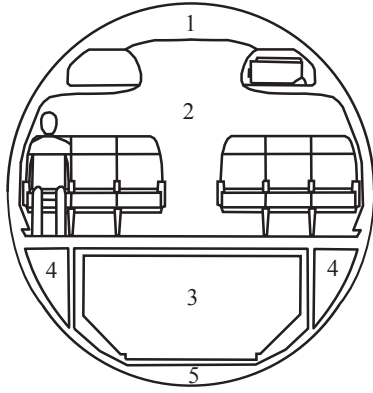


Figure 1: Compartments in a single aisle commercial aircraft (1. crown, 2. passenger cabin, 3. cargo bay, 4. triangle, 5. bilge)

was investigated to find the optimal configuration.

This article aims to demonstrate the effectiveness of a combined CFD and DoE methodology for the construction of models for the prediction of the heat transfer of thermally sensitive equipment placed in the confined compartments of commercial aircraft. The shift in industry to using greater levels of composite materials and the move towards an “all-electric” aircraft, which involves the replacement of hydraulic and pneumatic systems with electrical ones, will place increased pressure on thermal management systems [24]. It is therefore necessary for aircraft thermal designers to be able to generate models capable of accurately predicting the heat transfer that can occur in these confined compartments to ensure safe and reliable operation of the installed systems by locating them in positions of optimal heat transfer.

This study focuses on the applied case of the heat transfer and flow fields in the crown compartment in the fuselage of a single aisle commercial aircraft. The crown compartment is defined as the confined area between the passenger cabin and the external fuselage. See figure 1. The area corresponds to a complex configuration in terms of geometry, air volume, installed avionic systems and ventilation. This analysis deals with the time the aircraft is on the ground during turn around when systems are still operational and the fuselage experiences high skin temperature due to solar heating. This issue of adequate cabin cooling for aircraft while on the ground has been highlighted as a significant issue for the Airbus A380 by Aranjo et al. [4]. The combination of the climatic conditions and the aircrafts size leads to elevated temperatures in the cabin and thus requires additional power input from the APU.

This work forms part of the overall European FP7 funded MAAXIMUS (More Affordable Aircraft through eXtended, Integrated and Mature nUmerical Sizing) project. The project aims to develop a new methodology for the fast development and right-first-time validation of a highly optimised composite fuselage due to a coordinated effort between virtual structure development and composite tech-

nology. This work is part of the heat transfer section of the project which is developing heat transfer models for avionic components in aircraft compartments in the next generation of commercial aircraft.

Nomenclature

| | |
|--------------|--|
| A | Area (m^2) |
| c_p | Specific heat ($\text{Jkg}^{-1}\text{K}^{-1}$) |
| D | Dimensionality of CFD study (-) |
| D_{eff} | D-Optimal criterion (-) |
| E | Radiative flux (Wm^{-2}) |
| F | View Factor (-) |
| F_s | Safety factor (-) |
| g | Gravity (9.81ms^{-2}) |
| h | Convective heat transfer coefficient ($\text{Wm}^{-2}\text{K}^{-1}$) |
| J | Radiosity (Wm^{-2}) |
| k | Thermal conductivity ($\text{Wm}^{-1}\text{K}^{-1}$) |
| \dot{m} | Mass flow rate (kgs^{-1}) |
| N | Number of nodes in a mesh (-) |
| p | CFD order of discretisation accuracy (-) |
| q'' | Heat flux (Wm^{-2}) |
| R | Route G |
| R^2 | Coefficient of multiple determination (-) |
| r | Grid refinement factor (-) |
| S | SEPDC |
| T | Temperature (K) |
| \mathbf{X} | Regression matrix (-) |
| x | Regressor or input variable (-) |
| y | Response variable (-) |

Abbreviations

| | |
|------|---------------------------------|
| CFRP | Carbon fibre reinforced polymer |
| CL | Centreline |
| DoE | Design of Experiments |
| DP | Design point |
| GCI | Grid Convergence Index |
| PC | Polycarbonate |

Greek Symbols

| | |
|---------------|--|
| α | Coded input variable (-) |
| β | Regressor coefficient (-) |
| ε | Emissivity (-) |
| μ | Viscosity ($\text{kgm}^{-1}\text{s}^{-1}$) |
| ρ | Density (kgm^{-3}) |

Subscripts

| | |
|----------|---------------------------|
| b | bottom wall |
| $coarse$ | coarse grid |
| $fine$ | fine grid |
| fus | fuselage |
| in | inlet |
| l | left wall |
| r | right wall |
| rad | radiation |
| t | top wall |
| x, y | Cartesian coordinates (m) |

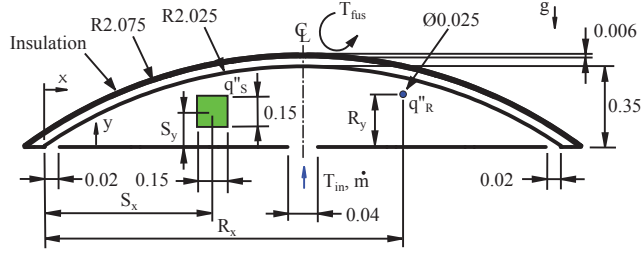


Figure 2: Populated crown compartment (dimensions in m, inlet and outlets not to scale)

2. Design of Experiments

Design of Experiments refers to the technique of planning an experiment so that appropriate data that can be analysed by statistical methods can be collected, resulting in valid and objective conclusions [17]. It is applicable to both physical processes and computer simulation models and is an effective tool for maximising the amount of information gained from a study while minimising the amount of data to be collected [26]. DoE methodologies have been used extensively in previous works for optimisation and process improvement purposes [8, 9, 19, 27].

The model of the crown compartment is presented schematically in figure 2. It consists of a circular segment with an inlet for the cabin ventilation system located on the centre of the floor and two outlets at either side of the compartment. There is a 50mm layer of insulation on the internal side of the fuselage. The two internal dissipating elements considered in this study are defined as the Secondary Electrical Power Distribution Centre (SEPDC) and the Route G. The SEPDC is a piece of avionic equipment which is mounted in the compartment and the Route G is an electrical conduit. The influence of mounting is not considered in this study.

The first step in the DoE process is to choose the list of input variables whose influence will affect the output response variable(s). Because the main aim of work is to determine the optimal location of the internal dissipating elements, their x and y locations were selected as input variables (see table 1). The heat fluxes of the two elements were fixed. The temperature of the fuselage due to solar heating has been chosen as an input variable. The mass flow rate and temperature of the cabin air conditioning were also fixed. There is a strong restriction on the mass flow rate and temperature of the cabin air conditioning system and its values cannot be altered as this would result in a significant decrease in efficiency for the onboard power systems. Therefore, this study has 5 input variables and they are listed in table 1. The x and y positions are measured from the centre-points of the dissipating elements. Distance from x -origin to the centreline (CL) is 1.138m.

Table 1 also presents the lower and upper limits of the input variables. These are simply the minimum and maximum values allowed. However, due to the shape of the

Table 1: Input variables

| Symbol | x_i | Min. limit | Max. limit |
|-----------|-------|------------|------------|
| S_x | x_1 | 0.375m | 1.901m |
| S_y | x_2 | 0.075m | 0.25m |
| R_x | x_3 | 0.15m | 2.126m |
| R_y | x_4 | 0.0375m | 0.3125m |
| T_{fus} | x_5 | 323.15K | 378.15K |

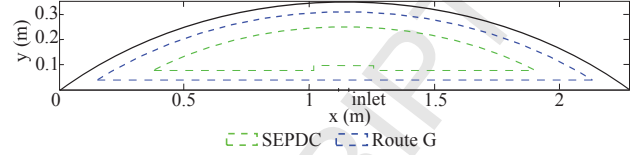


Figure 3: Boundary constraints

crown compartment, i.e. a circular segment, some combinations of the x and y positions of the dissipating elements can lie outside the physical geometry when the input test matrix is generated (e.g.: if $R_x = R_{x,max}$ and $R_y = R_{y,max}$). To overcome this issue, boundary constraints were created so this would not happen. A circular segment was defined for each of the dissipating elements where by design points for analysis could not be generated when their centre-points lie outside these boundaries. See figure 3.

The next step in the DoE process is to generate the input variable text matrix, \mathbf{X} , known as the regression matrix. From figure 3, it can be seen that the boundary constraint areas are also circular segments, meaning four of the five input variables are therefore “irregular” regions as they are not cubical or spherical. Because of this, standard designs are not the best choice. Standard designs methods, such as Central Composite Design and Box-Behnken Design, work best for cubical and spherical regions [17]. When \mathbf{X} is generated with either of these models, it leads to numerous points outside the physical geometry and positions where the dissipating elements overlap.

Computer-generated designs are an alternative approach. These types of design are known as “Optimal Designs”. By an optimal design, it means a design is “best” with respect to some criterion. Computer programs are required to construct these designs. In this work, the Matlab Model-Based Calibration toolbox was used. The optimality criterion chosen for this study is the most widely used criteria called the D-optimality criterion [17]. A D-Optimal design aims to reduce the volume of the confidence region on the vector of regression coefficients [3]. The D-Optimality value is calculated from eq. 1

$$D_{eff} = \frac{\log_e(|\mathbf{X}'\mathbf{X}|)}{n} \quad (1)$$

where \mathbf{X} is the regression matrix and n is the number of terms in the regression matrix. Matlab iterates the values

Table 2: Design points

| DP | S_x (m) | S_y (m) | R_x (m) | R_y (m) | T_{fus} (K) |
|----|-----------|-----------|-----------|-----------|---------------|
| 1 | 0.4767 | 0.075 | 1.9509 | 0.0375 | 370.82 |
| 2 | 0.5786 | 0.075 | 0.2 | 0.0558 | 374.48 |
| 3 | 0.6802 | 0.145 | 2.076 | 0.0558 | 323.15 |
| 4 | 0.9854 | 0.075 | 0.8253 | 0.0375 | 323.15 |
| 5 | 0.9854 | 0.225 | 1.5757 | 0.2575 | 345.15 |
| 6 | 0.6802 | 0.125 | 0.9504 | 0.2942 | 370.82 |
| 7 | 1.5958 | 0.185 | 0.8253 | 0.1842 | 378.15 |
| 8 | 1.7993 | 0.095 | 1.9509 | 0.0925 | 326.82 |
| 9 | 1.7993 | 0.075 | 0.5752 | 0.2208 | 341.48 |
| 10 | 1.5958 | 0.085 | 0.9504 | 0.0375 | 378.15 |
| 11 | 1.3923 | 0.165 | 1.2005 | 0.2942 | 323.15 |
| 12 | 0.7819 | 0.165 | 1.7008 | 0.1292 | 378.15 |
| 13 | 0.6802 | 0.165 | 0.4501 | 0.1842 | 334.15 |
| 14 | 0.5785 | 0.145 | 0.9504 | 0.0375 | 356.15 |
| 15 | 1.6975 | 0.085 | 1.4507 | 0.2758 | 378.15 |
| 16 | 1.5958 | 0.185 | 2.076 | 0.0375 | 363.48 |
| 17 | 1.2906 | 0.225 | 1.0755 | 0.0925 | 323.15 |
| 18 | 1.5958 | 0.155 | 0.2 | 0.0375 | 345.15 |
| 19 | 0.8837 | 0.225 | 0.3251 | 0.0558 | 378.15 |
| 20 | 0.4767 | 0.075 | 1.4507 | 0.2208 | 323.15 |
| 21 | 1.4432 | 0.1725 | 1.3256 | 0.1613 | 343.40 |
| 22 | 1.138 | 0.125 | 1.138 | 0.23 | 350.65 |
| 23 | 1.138 | 0.15 | 1.35 | 0.14 | 350.65 |
| 24 | 1.138 | 0.15 | 1.926 | 0.14 | 350.65 |
| 25 | 1.138 | 0.15 | 1.138 | 0.0375 | 350.65 |
| 26 | 1.138 | 0.15 | 1.138 | 0.3125 | 350.65 |
| 27 | 1.138 | 0.125 | 1.138 | 0.23 | 323.15 |
| 28 | 1.138 | 0.125 | 1.138 | 0.25 | 378.15 |
| 29 | 1.2906 | 0.075 | 1.4535 | 0.0375 | 350.65 |
| 30 | 1.138 | 0.225 | 1.138 | 0.12 | 350.65 |
| 31 | 0.55 | 0.13 | 1.138 | 0.175 | 350.65 |
| 32 | 1.726 | 0.13 | 1.138 | 0.175 | 336.90 |
| 33 | 1.5195 | 0.1125 | 0.669 | 0.10625 | 336.90 |
| 34 | 0.7565 | 0.1125 | 1.607 | 0.10625 | 336.90 |

of \mathbf{X} until it finds the optimum D_{eff} value. The iteration process is setup as a maximisation problem so the value of D_{eff} grows with each iteration [3]. Table 2 shows the values of the input variables for the D-Optimal design of the crown compartment (DP 1 - 21). Some additional user-generated design points were added to improve the prediction and reduce the predicted error variance around the inlet (DP 22 - 34).

3. CFD Analysis

3.1. Geometry & Mesh

The geometry of the crown compartment was generated using the Ansys Design Modeler module in Ansys Workbench 13.0. The list of design parameters generated in the DoE stage was imported into Ansys Workbench to

conduct a parametric study. Ansys Workbench automatically generates the geometry of all the design points from the table of design parameters.

The mesh was constructed using the Ansys Workbench Meshing module. An All Triangles meshing method was used in the fluid region. This was due to problems with earlier meshing attempts using quadrilateral elements. The element quality was relatively poor, especially in areas close to the outlets where the circular arc of the insulation meets the straight line of the crown floor which generated highly skewed elements. Quadrilateral elements were used to mesh the insulation region. Refinements were included in the mesh to adequately resolve areas close to all the walls.

3.1.1. Grid Independence Study

To test that the results were independent of the mesh used, a grid convergence analysis was conducted. A coarse and fine grid was generated. The refinement factor r , defined by Roache [23] is

$$r = \left(\frac{N_{fine}}{N_{coarse}} \right)^{\frac{1}{D}} \quad (2)$$

where N is the number of nodes in the fine or coarse grids, and D is the dimensionality of the study, i.e. 2. Roache [23] stated that the minimum value to conduct a grid convergence analysis is $r \geq 1.3$. The coarse and fine grids generated had 12080 and 22079 nodes respectively. For the grid in this analysis $r = 1.352$.

The discretisation error was estimated using the popular Grid Convergence Index (GCI). For the fine grid, it is defined as

$$GCI = F_s \frac{|\xi|}{r^p - 1} \quad (3)$$

where F_s is the safety factor, p is the order of accuracy, and ξ is defined by

$$\xi = \frac{f_{coarse} - f_{fine}}{f_{fine}} \quad (4)$$

where f_{coarse} is a coarse grid solution and f_{fine} is a fine grid solution. For a two grid study, a value of $F_s = 3$ is recommended [22]. The concept of the GCI is to approximately relate the relative error ξ , calculated in eq. 4 produced by whatever grid convergence study (for any p and r) to the ξ that would be expected using a fine grid with a different p and r . For further details see Roache [23]. The GCI was calculated for the following parameters: the average fluid temperature, the average insulation surface temperature, the average SEPDC surface temperature, the average Route G surface temperature, the average temperature along the line $x = 1.538\text{m}$, and the temperature at $[x, y] \approx [0.1, 0.04]$. The values of GCI for all parameters were less than 3% which suggest the error associated with the grid discretisation is minimal.

Table 3: Solid thermal properties

| Mat. | Region | ρ (kg/m ³) | c_p (J/kg.K) | k (W/m.K) | ϵ (-) |
|------|----------|--------------------------------|-------------------|----------------|-------------------|
| Al | SEPDC | 2719 | 871 | 202.4 | 0.95 |
| | Route G | | | | |
| PC | Fuselage | 1300 | 1200 | 0.21 | 0.95 |
| | Floor | | | | |
| Ins. | Ins. | 180 | 840 | 0.05 | 0.95 |

3.2. Solution Setup

The solution was setup and solved using Ansys Fluent 13.0. The density-based, implicit, laminar and 2nd order upwind solvers were utilised. The Energy equation was activated to resolve temperatures. The Surface-to-Surface (S2S) radiation model was used to resolve radiation. This model assumes that any absorption, emission or scattering of radiation can be ignored, therefore only “surface-to-surface” radiation is considered in the analysis [1]. The model also assumes that all surface are diffuse emitters of radiation.

Air is the working fluid inside the crown compartment. It was assumed to be an incompressible ideal gas. The additional thermal properties of specific heat c_p , thermal conductivity k , and viscosity μ were temperature dependent. Thermal properties of solid materials are presented in table 3. Polycarbonate (PC) was selected as the material to represent CFRP in this study. The thermal properties of a CFRP used in the skin of an aircraft wing are defined by Peterson et al. [21] as $0.642 \text{ Wm}^{-1}\text{K}^{-1}$ for k and $1059 \text{ Jkg}^{-1}\text{K}^{-1}$ for c_p . These values are reasonably close to PC and means that it can be used as an approximation of the CFRP thermal behaviour.

The fuselage surface was setup as a wall boundary condition. To model the thickness of the material, a 1D conduction problem was included with the thickness of the wall specified as 6mm. The thermal boundary condition was set up as a constant temperature, where the applied temperature is a parameter in the DoE analysis, T_{fus} . See table 2 for the list of applied T_{fus} for each DP. The crown compartment floor is setup as an adiabatic wall. A constant velocity normal to the inlet of 0.15ms^{-1} was applied to replicate the cabin ventilation system. The temperature of this air, T_{in} , was defined as 290.15K. The two outlets were defined as pressure outlets. The insulation surface was defined as a coupled wall. No additional boundary conditions are required because the solver will calculate heat transfer from the solution in adjacent walls [2]. A constant heat flux was applied to all walls of the SEPDC with a value of $q''_S = 422.8\text{Wm}^{-2}$. The constant heat flux applied to the Route G surface was $q''_R = 77\text{Wm}^{-2}$. The solution was initialised at the inlet conditions.

The solution was set up and runs initially as a steady state problem. The solver is then switched to a transient one to capture any unsteadiness in the flow. Activating

time dependence is useful when solving steady state solutions which tend towards instability [2]. To determine when to change from steady state to transient solver, a number of different surface monitors were utilised. Five temperature monitors were created to observe the change in temperature as the iterations increase. The temperature monitors include those of the average fluid temperature, average insulation surface temperature, average SEPDC surface temperature, average Route G surface temperature and a point monitor located close to the outlet at $[x, y] \approx [0.1, 0.04]$. Monitors of the area weighted average of the wall shear stress on the crown floor were also used to determine steadiness. When the change in monitors becomes approximately constant, the solution is deemed steady so the solver is switched to the transient one. A time step of 0.01s was used for the transient time step size. The solution was iterated again until the values of the monitors remain approximately constant with increasing time and values of the residuals of continuity, momentum and energy equations are of the order of 10^{-6} . Models were run on a computer with a 4 core processor with a speed of 2.67GHz and 8GB of RAM.

4. Regression Analysis

4.1. Model

When there is a single dependent variable or response y that depends on k independent or regressor variables, x_1, x_2, \dots, x_k , the relationship between these variables can be characterised by a mathematical model called a regression model. The regression model is built from a set of sample data [17]. The model being used in this study is a quadratic model with five variables. This considers interaction terms and is given by

$$y = \beta_0 + \sum_{i=1}^k \beta_i x_i + \sum_{i=1}^k \beta_{i,i} x_i^2 + \sum_{i<j} \beta_{i,j} x_i x_j + \epsilon \quad (5)$$

where $k = 5$ and ϵ is the error term. If the quadratic terms for eq. 5 are rewritten such that $x_{k+1} = S_x^2$, $x_{k+2} = S_x S_y$, \dots , $x_{20} = T_{fus}^2$ and $\beta_{k+1} = \beta_{1,1}$, $\beta_{k+2} = \beta_{1,2}$, \dots , $\beta_{20} = \beta_{5,5}$, then eq. 5 can be written as a linear regression model

$$y = \beta_0 + \beta_1 x_1 + \beta_2 x_2 + \dots + \beta_{20} x_{20} + \epsilon \quad (6)$$

Writing this equation in terms of the design point observations, it is then

$$\begin{aligned} y_{DP} &= \beta_0 + \beta_1 x_{DP,1} + \beta_2 x_{DP,2} + \dots + \beta_{20} x_{DP,20} + \epsilon_{DP} \\ &= \beta_0 + \sum_{j=1}^{20} \beta_j x_{DP,j} + \epsilon_{DP} \quad DP = 1, 2, \dots, 34 \end{aligned} \quad (7)$$

The model terms in eq. 7 may be written in matrix notation as

$$\mathbf{y} = \mathbf{X}\beta + \epsilon \quad (8)$$

where

$$\mathbf{y} = \begin{bmatrix} y_1 \\ y_2 \\ \vdots \\ y_{DP} \end{bmatrix}, \quad \mathbf{X} = \begin{bmatrix} 1 & x_{1,1} & x_{1,2} & \cdots & x_{1,20} \\ 1 & x_{2,1} & x_{2,2} & \cdots & x_{2,20} \\ \vdots & \vdots & \vdots & & \vdots \\ 1 & x_{DP,1} & x_{DP,2} & \cdots & x_{DP,20} \end{bmatrix},$$

$$\beta = \begin{bmatrix} \beta_1 \\ \beta_2 \\ \vdots \\ \beta_{DP} \end{bmatrix} \quad \text{and} \quad \epsilon = \begin{bmatrix} \epsilon_1 \\ \epsilon_2 \\ \vdots \\ \epsilon_{DP} \end{bmatrix}$$

The method of least squares is used to calculate the values of β so that the sum of the square of the errors ϵ is minimised. The fitted regression model for a point i is

$$\hat{y}_i = \hat{\beta}_0 + \sum_{j=1}^{20} \hat{\beta}_j x_{i,j} \quad (9)$$

For a complete description of regression analysis and response surface analysis see Montgomery [17] and Khuri and Cornell [13].

4.2. Response variables

The convective heat transfer coefficients of the dissipating element surfaces were selected as response variables. h is calculated from

$$h = \frac{q'' - q''_{rad}}{T - T_\infty} \quad (10)$$

where q''_{rad} is the radiative heat flux, T is the average surface temperature and T_∞ is the reference temperature which is defined as the inlet temperature T_{in} . To calculate q''_{rad} , the thermal resistance network was defined for the geometry. A radiosity node was placed on each surface except for the input and outputs which were assumed non-participating. Applying energy conservation at each node, then the net heat transfer from any one surface i must be equal to the sum of the net radiation to each of the other surfaces j ,

$$\frac{E_i - J_i}{\left(\frac{1-\varepsilon_i}{\varepsilon_i A_i}\right)} = \sum_j \left(\frac{J_i - J_j}{\left(\frac{1}{A_i F_{i,j}}\right)} \right) \quad (11)$$

where ε is the emissivity, J is the radiosity, F is the view factor from one surface to another, A is the heat transfer surface area, and E is the radiative flux. The view factors for each design point were calculated by Fluent. Eq. 11 can be re-written for the i^{th} equation as

$$J_i - (1 - \varepsilon_i) \sum_j (F_{i,j} J_j) = \varepsilon_i E_i \quad (12)$$

which generated the same number of equations as surfaces which can then be solved simultaneously to find the values of J . When all these values are found, the heat transfer coefficients in eq. 10 can be calculated.

4.3. Fitted Regression Models

The Matlab Model-Based Calibration toolbox was used for building the fitted regression models from the CFD data from each DP. These results are presented and discussed in this section.

4.3.1. SEPDC right wall ($h_{S,r}$)

Figure 4 presents the contour plot for $h_{S,r}$ for S_x versus S_y . The boundary constraints discussed in section 2 have been fitted to the contour plots as they represent the physical bounds in which the results are relevant. It is also important to note that for the contour plots, the 3 other input variables not displayed are set to their average values. Hence some overlap of the internal dissipating elements can occur, but they have been included as the best method of graphically representing the results. Figure 4a shows that for the SEPDC right wall, the values of h increase as S_x decreases, and decrease as S_x increases. This is due to the fact that the cold air from the inlet comes in direct contact with this surface when $S_x < \text{CL}$. For $S_x > \text{CL}$, the hot air from the SEPDC becomes trapped between the SEPDC and the insulation resulting in increased fluid temperatures. It can also be seen that as S_y increases, the h also decreases, resulting from the hot buoyant air becoming trapped between the SEPDC and the insulation in this region.

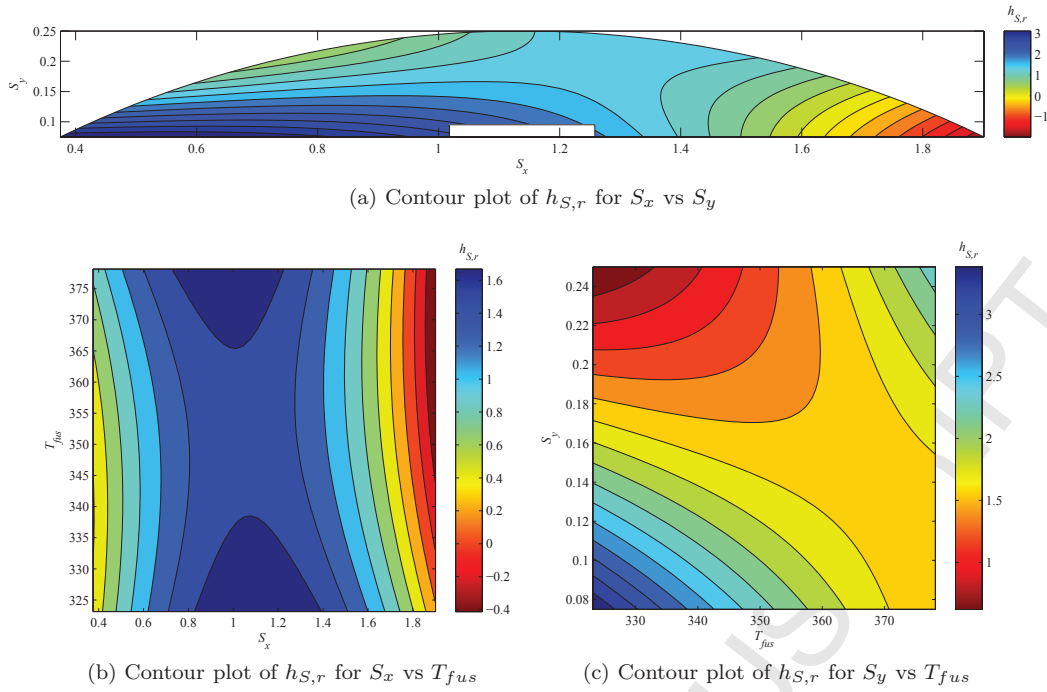
Figures 4b and 4c show the influence the fuselage temperature has on the SEPDC location. This is mainly due to the increased air temperature and the corresponding effect on the penetration of the plume into the fluid. Figure 4b shows that for the lowest values of T_{fus} , the highest values of h are generated. As T_{fus} increases the lowest values of h are generated when the SEPDC is closest to the right hand side of the compartment. Figure 4c shows that the highest values of h are generated at the lowest values of S_y and T_{fus} as the SEPDC is closest to the inlet. Overall it was found that the Route G had little influence on the SEPDC.

An important observation to note in the results is the negative values of h . These values are generated for cases where the surface receives heat rather than dissipating heat. The heat balances for these cases show that there is greater heat flux going to the surface compared to the heat flux leaving the surface.

4.3.2. SEPDC left wall ($h_{S,l}$)

Figure 5a presents the contour plot of $h_{S,l}$ for S_x versus S_y . It can be observed that it is more-or-less the mirror image of figure 4a for the right wall. The lowest values of h are generated when $S_x > \text{CL}$, and the lowest values are produced when $S_x < \text{CL}$. Again lower values of h are seen when S_y increases.

For figures 5b and 5c it is noted that the contours take a slightly different shape to those of figures 4b and 4c but they still predict similar values of h for the some input values. This problem is due to the fact the model finds

Figure 4: Contour plots of $h_{S,r}$

it harder to predict results when the SEPDC is located *very close* to the inlet as there is the possibility for such variation in this region. There is a significant change in flow and thermal structures with slight change in input variables. This effect had tried to be accounted for earlier in the work by adding additional design points close to the inlet. However, as stated above, the values of h predicted for the left wall are still similar to the right wall, with the highest values of h for lowest values of S_x and T_{fus} (figure 5b) and the highest values of h when T_{fus} and S_y are minimised (figure 5c).

4.3.3. SEPDC top wall ($h_{S,t}$)

Figure 6 shows the contour plot of h for SEPDC position inside the crown compartment. The highest values of h are produced when S_x is closest to the inlet and S_y is low. The values of h decrease as S_y increases.

4.3.4. SEPDC bottom wall ($h_{S,b}$)

Figure 7a displays the contours of h for the SEPDC position. It can be seen that the location that results in the highest value of h is directly above or around the inlet. As the distances are moved further from the inlet, the value of h decreases.

Figure 7b again shows that the highest values of h are achieved directly above the inlet. As the SEPDC is moved away from the inlet in either direction, a decrease in h is seen. Increase in temperature of the fuselage also causes further decrease in h . In figure 7c the minimum T_{fus} and S_y result in the highest values of h . Increasing either of these variables results in a general decrease in h as they

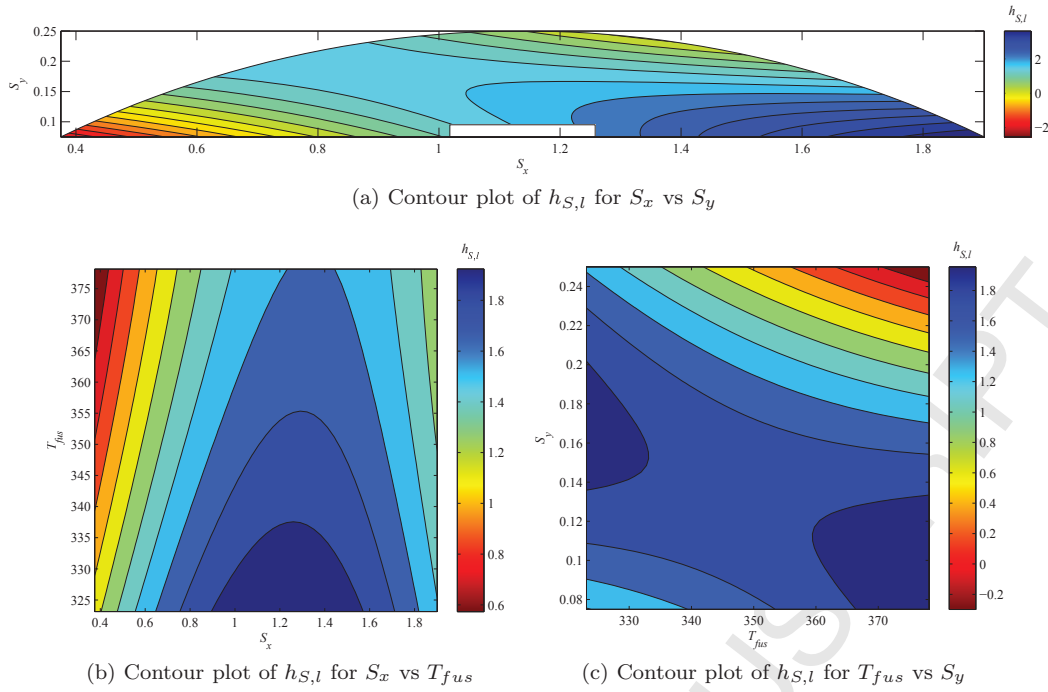
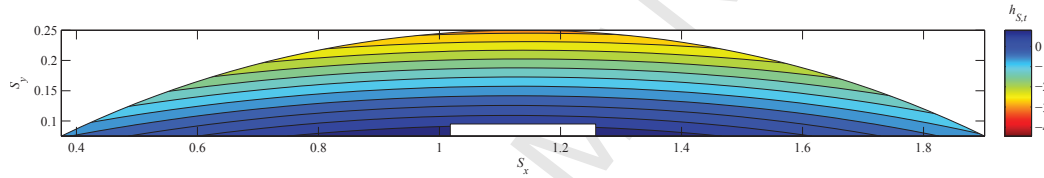
in turn influence the effect of the inlet flow on the bottom surface.

4.3.5. Route G (h_R)

Figure 8a shows the h of the Route G based on its location. The largest values of h are generated when the element is located close to the crown floor. The values decrease as R_y is increased. The magnitude of the change however is relatively small and the R_x and R_y parameters have little effect when compared to the other input parameters in figure 8.

For figure 8b, it can be seen that for the lower values of R_x and T_{fus} that the h is maximised. The values of h do not vary very much with change in R_x , similar to figure 8a. For the case of T_{fus} and R_y in figure 8c, h is minimised when R_y is kept as close to the fuselage as possible. The lowest values of h occur when the Route G is close to the fuselage and T_{fus} is high.

Figures 8d and 8e look at the influence of the SEPDC position and the fuselage temperature on h of the Route G. A reminder is necessary here about the statement earlier that for all contour plots, the variables not shown in each plot are set to the average value. Hence, the Route G is located in the centre of the compartment. For figure 8d the SEPDC is located below the Route G so this is why the lowest values of h are observed at the CL, and why they decrease as the SEPDC is moved away. Similarly, for figure 8e, the Route G is located centrally. At the lowest values of S_y , the SEPDC is located below the Route G and is thus in its plume. As S_y increases, the SEPDC moves into a position above the Route G resulting in a drop in h . Figure 8f highlights again the dominance of the SEPDC

Figure 5: Contour plots of $h_{S,l}$ Figure 6: Contour plot of $h_{S,t}$ for S_x vs S_y

on the thermal structures inside the compartment. This figure shows that to minimise h_R , the Route G needs to be the furthest distance possible from the SEPDC.

4.4. Regressor Coefficients

The regressor coefficients for the coded input variables calculated for the fitted regression models are presented in table 4. The coded input variables are expressed as a value from -1 to +1 where -1 is the minimum limit and +1 is the maximum limit. They are calculated from

$$\alpha_i = \frac{x_i - (x_{min} + x_{max})/2}{(x_{max} - x_{min})/2} \quad (13)$$

This then allows for the prediction of any of the response variables for a given set of input variables,

$$\hat{y}_i = \hat{\beta}_0 + \sum_{j=1}^{20} \hat{\beta}_j \alpha_{i,j} \quad (14)$$

The Goodness of Fit of each model is also presented in table 4 using the coefficient of multiple determination statistic R^2 . This is a measure of how successful the fit is in explaining variation in the data. R^2 value can range

between 0 and 1, where a value closer to 1 indicating that a greater proportion of variance is accounted for by the model. It can be seen that it ranges from 0.878 - 0.978 meaning that the models fit the data well.

5. Conclusions

Fitted regression models have been built from CFD simulations of the populated crown compartment. These models allow for the prediction of the convection heat transfer coefficients on the surfaces of the compartments internal dissipating elements based on their positions and the external surface temperature of the fuselage. They can be used at the design stage of an aircraft to find the optimal placement in terms of heat transfer. Overall, it has been found that the optimal positions of the SEPDC and Route G are when they are located as close to the crown floor as possible without completely blocking the air flow. In these positions, most of the surfaces of the elements come in direct contact with the cooler inlet air flow.

The methodology employed, i.e. combined DoE, CFD and regression techniques, allows aircraft thermal engineers to optimise equipment placement during the design

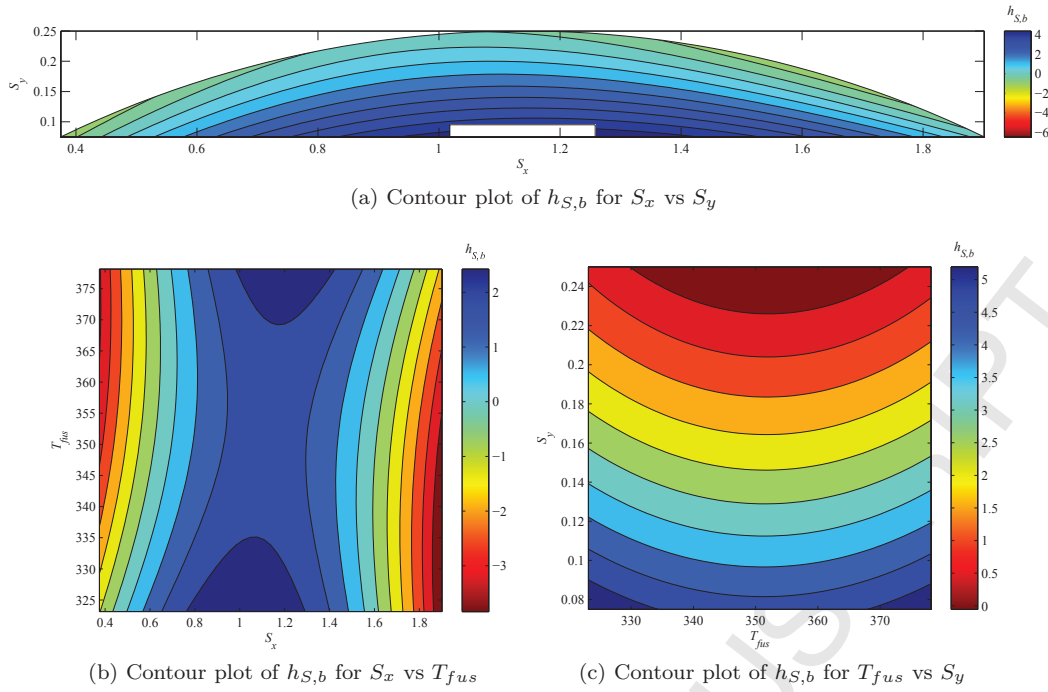
Figure 7: Contour plots of $h_{S,b}$

Table 4: Regressor coefficients

| β_j | $h_{S,r}$ | $h_{S,l}$ | $h_{S,t}$ | $h_{S,b}$ | h_R |
|--------------|-----------|-----------|-----------|-----------|--------|
| β_0 | 1.588 | 1.795 | -0.709 | 2.096 | 0.221 |
| β_1 | -0.376 | 0.266 | -0.042 | -0.315 | -0.887 |
| β_2 | -0.527 | -0.569 | -1.988 | -2.477 | 0.082 |
| β_3 | 0.271 | -0.136 | 0.136 | 1.120 | 0.056 |
| β_4 | 0.071 | -0.115 | 0.058 | -0.249 | -1.689 |
| β_5 | -0.056 | -0.214 | -0.243 | -0.058 | -0.113 |
| β_6 | -1.513 | -0.686 | -1.581 | -5.203 | 0.998 |
| β_7 | 2.102 | -2.670 | 0.085 | -0.909 | -1.708 |
| β_8 | 0.759 | -0.218 | -0.337 | 1.941 | -2.210 |
| β_9 | 0.083 | -0.378 | 0.087 | -1.049 | -1.244 |
| β_{10} | -0.265 | 0.095 | -0.114 | 1.206 | 0.862 |
| β_{11} | 0.218 | -0.682 | -0.124 | 0.328 | 0.211 |
| β_{12} | -0.415 | -0.233 | 0.278 | 0.844 | -1.354 |
| β_{13} | 0.981 | -0.110 | -0.126 | -0.614 | -0.697 |
| β_{14} | 0.946 | -0.668 | -0.084 | -0.028 | -0.929 |
| β_{15} | 0.067 | -0.396 | 0.054 | -0.441 | -0.916 |
| β_{16} | 0.693 | -0.616 | -0.080 | 1.796 | -0.843 |
| β_{17} | 0.407 | -0.182 | 0.047 | -0.706 | -0.033 |
| β_{18} | 0.203 | 0.038 | -0.021 | -0.323 | 1.333 |
| β_{19} | 0.520 | -0.107 | -0.071 | 0.118 | -0.932 |
| β_{20} | 0.231 | 0.039 | 0.059 | 0.790 | -0.311 |
| R^2 | 0.978 | 0.958 | 0.977 | 0.885 | 0.878 |

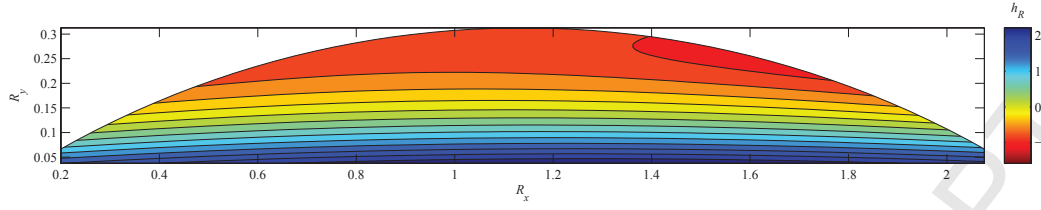
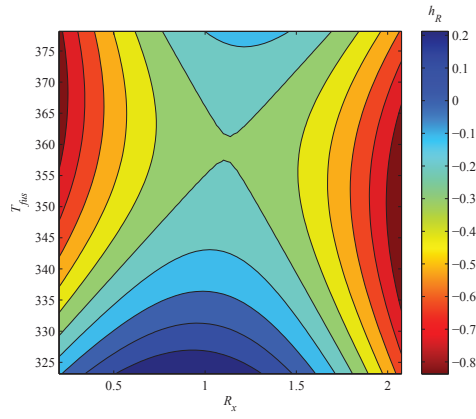
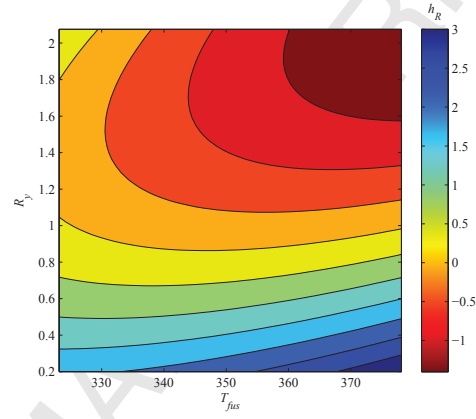
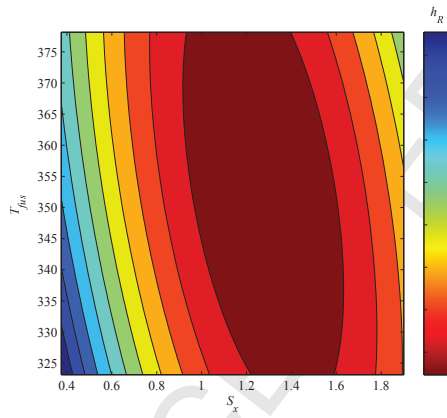
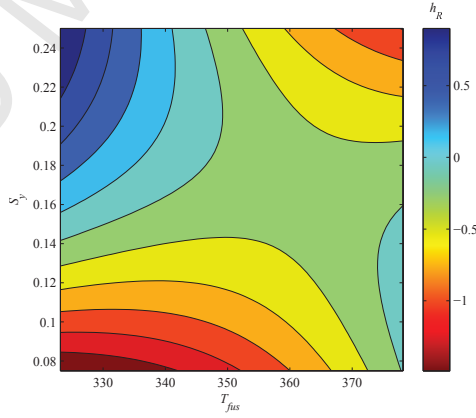
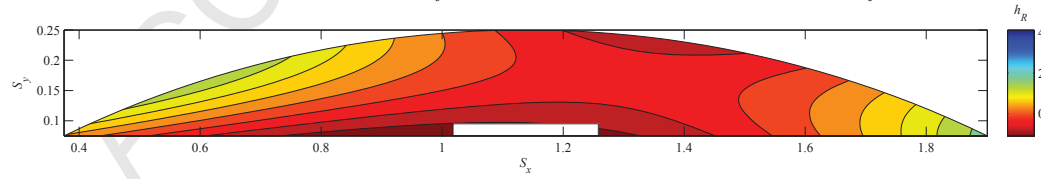
phase of the aircraft. The determined models should be incorporated into global aircraft numerical models to improve accuracy and reduce model size and computational time. It should also be applied to the other confined compartments, i.e. triangles and bilge, to evaluate and optimise equipment placement in these areas.

Funding Source

The research leading to these results has received funding from the European Community's Seventh Framework Programme FP7 2007 - 2013 under grant agreement No. 213371, MAAXIMUS (www.maaximus.eu).

References

- [1] Ansys Fluent Theory Guide, Ansys Inc., Canonsburg, PA, USA, 13.0 edition, 2010.
- [2] Ansys Fluent User's Guide, Ansys Inc., Canonsburg, PA, USA, 13.0 edition, 2010.
- [3] Model-Based Calibration Toolbox: Model Browser User's Guide, The Mathworks Inc., Natick, MA, USA, 4.3 edition, 2011.
- [4] B.S. Arango, B.R. Hughes, H.N. Chaudry, Performance investigation of ground cooling for the Airbus A380 in the United Arab Emirates, *Appl. Therm. Eng.* 36 (2012) 87–95.
- [5] A. Baker, S. Dutton, D. Kelly, *Composite Materials for Aircraft Structures*, AIAA, Inc., VA, USA, 2nd edition, 2004.
- [6] V. Bianco, O. Manca, S. Nardini, M. Roma, Numerical investigation of transient thermal and fluiddynamic fields in an executive aircraft cabin, *Appl. Therm. Eng.* 29 (2009) 3418–3425.
- [7] R. Coquard, D. Baillis, M. Thomas, B. Estebe, Modeling of heat transfer across porous honeycomb structures, *J. Porous Media* 15 (2012) 647–663.

(a) Contour plot of h_R for R_x vs R_y (b) Contour plot of h_R for R_x vs T_{fus} (c) Contour plot of h_R for T_{fus} vs R_y (d) Contour plot of h_R for S_x vs T_{fus} (e) Contour plot of h_R for T_{fus} vs S_y (f) Contour plot of h_R for S_x vs S_y Figure 8: Contour plots of h_R

- [8] P. Frawley, J. Corish, A. Niven, M. Geron, Combination of CFD and DOE to analyse solid particle erosion in elbows, *Int. J. Comput. Fluid Dyn.* 23 (2009) 411–426.
- [9] P. Frawley, M. Geron, Combination of CFD and DOE to Analyze and Improve the Mass Flow Rate in Urinary Catheters, *J. Biomech. Eng.* 131 (2009) 084501.
- [10] G. Günther, J. Bosbach, J. Pennecot, C. Wagner, T. Lerche, I. Gores, Experimental and numerical simulations of idealized aircraft cabin flows, *Aerosp. Sci. Technol.* 10 (2006) 563–573.
- [11] J. Gupta, C.H. Lina, Q. Chen, Transport of expiratory droplets in an aircraft cabin, *Indoor Air* 21 (2011) 3–11.
- [12] A. Kelly, Very stiff fibres woven into engineering’s future: a long-term perspective, *J. Mater. Sci.* 43 (2008) 6578–6585.
- [13] A. Khuri, J. Cornell, *Response Surfaces: Designs and Analyses*, Marcel Dekker, Inc., New York, 2nd edition, 1996.
- [14] M. Kühn, J. Bosbach, C. Wagner, Experimental parametric study of forced and mixed convection in a passenger aircraft cabin mock-up, *Build. Environ.* 44 (2009) 961 – 970.
- [15] W. Liu, S. Mazumdar, Z. Zhang, S.B. Possou, J. Liu, C.H. Lin, Q. Chen, State-of-the-art methods for studying air distributions in commercial airliner cabins, *Build. Environ.* 47 (2012) 5–12.
- [16] V. Mellert, I. Baumann, N. Freese, R. Weber, Impact of sound and vibration on health, travel comfort and performance of flight attendants and pilots, *Aerosp. Sci. Technol.* 12 (2008) 18–25.
- [17] D. Montgomery, *Design of Experiments*, John Wiley & Sons, Inc., New York, 5th edition, 2001.
- [18] D. Moore, D. Newport, V. Egan, V. Lacarac, Ventilation and internal structure effects on naturally induced flows in a static aircraft wing, *Appl. Therm. Eng.* 32 (2012) 49–58.
- [19] A. Omran, B. Newman, D. Landman, Global aircraft aeropropulsive linear parameter-varying model using design of experiments, *Aerosp. Sci. Technol.* 22 (2012) 31–44.
- [20] M. Ostergaard, A. Ibbotson, O. Roux, A. Prior, Virtual testing of aircraft structures, *CEAS Aeronaut. J.* 1 (2011) 83–103.
- [21] D. Peterson, R. Rolfes, R. Zimmermann, Thermo-mechanical design aspects for primary composite structures of large transport aircraft, *Aerosp. Sci. Technol.* 5 (2001) 135–146.
- [22] P. Roache, Quantification of uncertainty in computational fluid dynamics, *Annu. Rev. Fluid Mech.* 29 (1997) 123–160.
- [23] P. Roache, *Verification and Validation in Computational Science and Engineering*, Hermosa Publishers, Albuquerque, NM, USA, 1998.
- [24] J. Rosero, J.A. Ortega, E. Aldabas, L. Romeral, Moving towards a more electric aircraft, *Aerosp. Electron. Syst. Mag., IEEE* 22 (2007) 3–9.
- [25] C. Soutis, Fibre reinforced composites in aircraft construction, *Prog. Aerosp. Sci.* 41 (2005) 143–151.
- [26] J. Telford, A brief introduction to design of experiments, *John Hopkins APL Tech. Dig.* 27 (2007) 224–232.
- [27] J. Zhang, H.y. Li, Y.z. Luo, G.j. Tang, Error analysis for rendezvous phasing orbital control using design of experiments, *Aerosp. Sci. Technol.* 17 (2012) 74–82.